

Reconciling the ionic and covalent pictures in rare-earth nickelates

Julien Varignon,¹ Mathieu N. Grisolia,¹ Jorge
Íñiguez,² Agnès Barthélémy,¹ and Manuel Bibes¹

¹*Unité Mixte de Physique, CNRS, Thales,
Université Paris Sud, Université Paris-Saclay,
1 avenue A. Fresnel, 91767, Palaiseau, France**

²*Materials Research and Technology Department,
Luxembourg Institute of Science and Technology (LIST),
5 avenue des Hauts-Fourneaux, L-4362 Esch/Alzette, Luxembourg*

(Dated: December 4, 2018)

The properties of AMO_3 perovskite oxides, where M is a 3d transition metal, depend strongly on the level of covalency between the metal d and oxygen p orbitals. With their complex spin orders and metal-insulator transition, rare-earth nickelates verge between dominantly ionic and covalent characters. Accordingly, the nature of their ground state is highly debated. Here, we reconcile the ionic and covalent visions of the insulating state of nickelates. Through first-principles calculations, we show that it is reminiscent of the ionic charge disproportionation picture (with strictly low-spin 4+ and high-spin 2+ Ni sites) while exhibiting strong covalence effects with oxygen electrons shifted toward the depleted Ni cations, mimicking a configuration with identical Ni sites. Our results further hint at strategies to control electronic and magnetic phases of transition metal oxide perovskites.

Transition metal oxides with an AMO_3 perovskite structure have attracted widespread interest over the last decades, both from academic and industrial points of view. This can be ascribed to their wide range of functionalities that originates from the interplay between lattice, electronic, and magnetic degrees of freedom [1]. Among all perovskites, rare-earth nickelates $R^{3+}Ni^{3+}O_3$ ($R=Lu-La, Y$) might be considered as a prototypical case because they possess almost all possible degrees of freedom present in these materials. Nickelates were intensively studied during the nineties [2, 3] and have regained interest in the few last years due to their great potential for engineering novel electronic and magnetic states [4–11].

Except for $R=La$, all rare-earth nickelates undergo a metal-insulator phase transition (MIT) at a temperature T_{MI} , accompanied by a symmetry lowering from $Pbnm$ to $P2_1/n$ [2, 3]. In this $P2_1/n$ phase, a Ni-site splitting is observed; this is usually associated with the appearance of charge disproportionation [12–14] from $2Ni^{3+}$ to $Ni^{(3+\delta)+} + Ni^{(3-\delta)+}$ and/or a breathing distortion of O_6 octahedra that leads to a rock-salt-like pattern of small and large NiO_6 groups [13]. At $T_N \leq T_{MI}$, nickelates undergo an antiferromagnetic (AFM) phase transition yielding a quadrupling of the magnetic unit cell ($\vec{k}=(\frac{1}{2}, 0, \frac{1}{2})$ with respect to the $Pbnm$ primitive cell) and possible collinear or non collinear spin orderings [15–18]. The electronic structure is also characterized by strong overlaps between O-2p and Ni-3d states leading to large covalent effects [2]. As a consequence, external stimuli, such as temperature, or chemical or hydrostatic pressure, can modify the electronic bandwidth and influence the MIT [19–22]. Efforts have thus been devoted to search for novel electronic phases in nickelates, mainly using strain engineering or confinement [10, 11, 23–25].

In spite of all these research efforts, the structural, electronic and magnetic properties of the bulk ground state are still under debate. This can be ascribed to the scarcity of systematic bulk studies, from both the experimental and theoretical sides. On one hand, bulk nickelates are hard to synthesize and mainly thin films have been studied [3]. On the other hand, no theoretical systematic studies have been performed due to the difficulty of reproducing the $RNiO_3$ ground state using density functional theory (DFT). In the context of DFT-based calculations, the choice of the Hubbard U correction for Ni-3d levels remains ambiguous; indeed, a great diversity of values, ranging from very weak to quite strong corrections, have been proposed and argued for in different works [5, 24, 26–29]. Moreover, the identified ground state is usually ferromagnetic [24, 26, 30], in contrast to the established antiferromagnetic ordering.

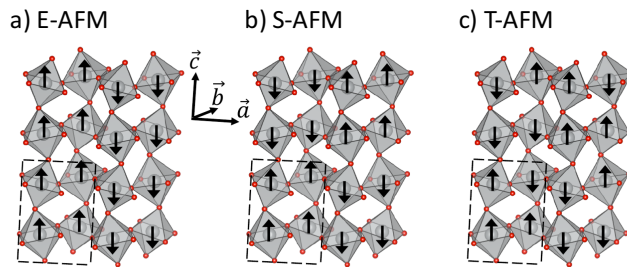


FIG. 1. **Sketch of the three complex antiferromagnetic orderings used in the calculations.** (a) E-type AFM ordering. (b) S-type AFM ordering. (c) T-type AFM ordering. The A cations are not displayed for clarity. The dashed lines represent the size of the crystallographic unit cell.

Here we performed a systematic study of various representative nickelates using the standard DFT+U formalism. We find that a small Coulombian correction on Ni-3d states is appropriate to reproduce the key ground state properties of these compounds. We then use this theory to discuss the electronic ground state of the nickelates, revealing the co-existence of ionic (Ni electronic states featuring a complete and strict charge disproportionation) and covalent (oxygen- p electrons shared with the charge-depleted Ni cations) features, and providing an unified picture of these materials that is easy to reconcile with existing (and apparently conflicting) proposals in the literature. Finally, we unveil a new pathway to control electronic and magnetic phases in perovskites by tuning the level of covalency.

RESULTS

Structural properties

First, we performed full geometry relaxations considering 80-atom supercells of both possible $Pbnm$ and $P2_1/n$ structures with different magnetic orderings: ferromagnetic (FM) as well as complex E-, S-, and T-type AFM orderings [5] based on $\uparrow\downarrow\downarrow$ spin chains in the (ab)-plane with different stackings along the \vec{c} axis (see Figures 1.a, b and c). We employed the PBEsol functional [31] in combination with a U correction [32] of 2 eV on Ni-3d states in order to account for electronic correlations. Several nickelates ($R=Y, Dy, Tb, Gd, Eu, Sm, Nd, \text{ and } Pr$) were considered, covering the phase diagram as a function

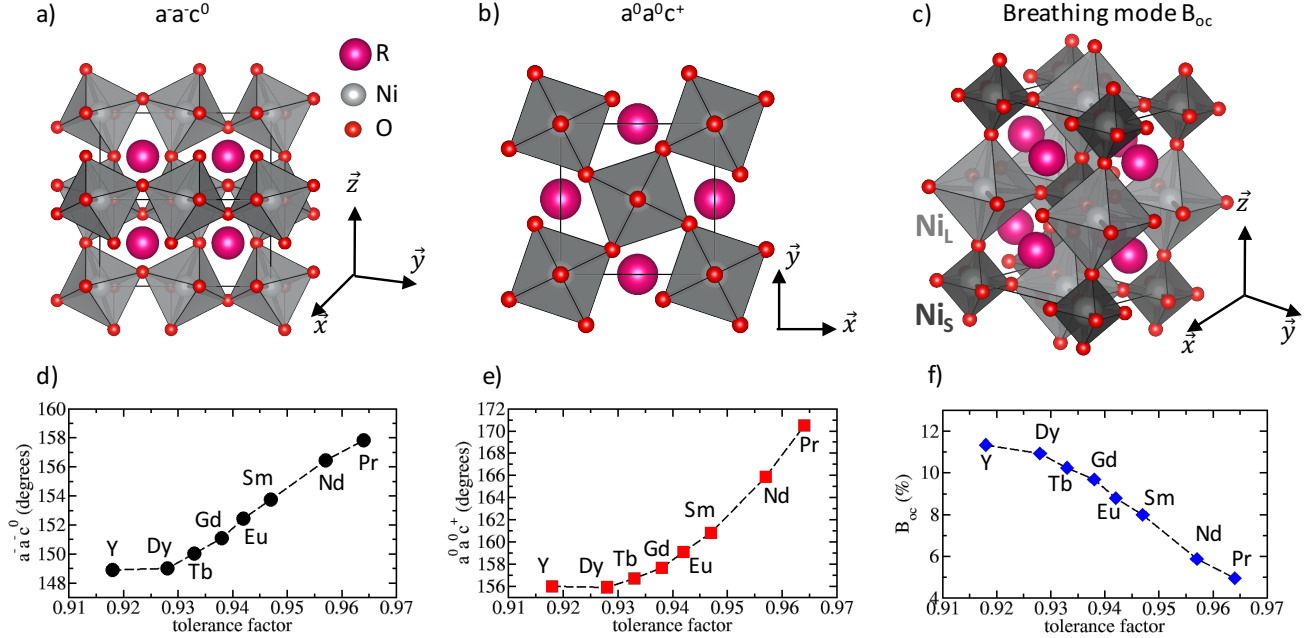


FIG. 2. **Rare-earth nickelates ground state structural properties.** (a), (b) and (c) Schematic pictures of the three main lattice distortions appearing in the ground state of nickelates: $a^-a^-c^0$ antiferrodistortive motion, $a^0a^0c^+$ antiferrodistortive motion and breathing of the oxygen cage octahedra B_{oc} . (d) and (e) Ni-O-Ni angle (in degrees) produced by the $a^-a^-c^0$ and $a^0a^0c^+$ antiferrodistortive motions. (f) Oxygen cage octahedra volume expansion/contraction (in %) produced by the breathing mode.

of rare-earth radius. All nickelates relax to a $P2_1/n$ insulating ground state with complex antiferromagnetic structures (S- or T-type depending on the rare-earth) and band gaps compatible with experiments [33, 34] (see Table I). All our $Pbnm$ phases favor a metallic FM solution [35]. We checked the reliability of our DFT+U calculations by changing the U correction to either 0 eV or 5 eV in SmNiO_3 . While the ground state is unchanged when no U-correction is applied [36], imposing $U = 5$ eV yields a $P2_1/n$ ferromagnetic and insulating solution that is much more stable than the considered complex AFM orderings ($\Delta E \simeq 160$ meV per 80-atom unit cell). This further supports our choice of a relatively small Hubbard correction for the Ni-3d electrons.

Our optimized ground state structures are characterized by three main lattice distortions. First, they feature two antiferrodistortive (AFD) modes that can be described, respectively, as $a^-a^-c^0$ and $a^0a^0c^+$ patterns using Glazer's notation [37]. These AFD modes are the

R	$\Delta E(\text{E-AFM})$	$\Delta E(\text{S-AFM})$	$\Delta E(\text{T-AFM})$	gap (eV)
Pr	-266	-393	-384	0.49
Nd	-172	-290	-282	0.50
Sm	-71	-139	-145	0.54
Eu	-35	-82	-92	0.56
Gd	-15	-51	-34	0.55
Tb	-9	-33	-13	0.58
Dy	-6	-10	13	0.59
Y	-4	-20	3	0.61

TABLE I. **Key quantities of the different relaxed ground states.** Computed energy differences ΔE (in meV per 80-atom unit cell) between the complex antiferromagnetic and ferromagnetic solutions and electronic band gap of the identified ground state.

main features of the phase with $Pbnm$ symmetry. Second, we have a breathing of the O_6 octahedra, B_{oc} (see Figures 2.a, b and c). The breathing mode only appears in the $P2_1/n$ symmetry and produces a rock-salt pattern of small and large NiO_6 groups, automatically resulting in two different Ni sites (see Figure 2.c). In the following we will use the notation Ni_S and Ni_L to refer to the Ni cations belonging to the small and large NiO_6 groups, respectively.

As usual in perovskites, the magnitude of the metal-oxygen-metal bond angles associated with the O_6 rotations is governed by steric effects (see Figures 2.d and e), and nickelates with low tolerance factors (*i.e.*, smaller R cations) [38] are more distorted. The alternating expansion/contraction pattern of the oxygen cage associated with the B_{oc} breathing also appears to be modulated by the rare earth (see Figure 2.f), as smaller R cations yield larger distortions. Finally, we observe a Jahn-Teller distortion in the ground state that is one to two orders of magnitude smaller than the breathing mode or the two AFD motions. Hence, the relaxed structures indicate that there is no significant orbital order in these systems, although the $3d^7 t_{2g}^6 e_g^1$ electronic configuration of Ni^{3+} in the high temperature $Pbnm$ phase is nominally Jahn-Teller active [28].

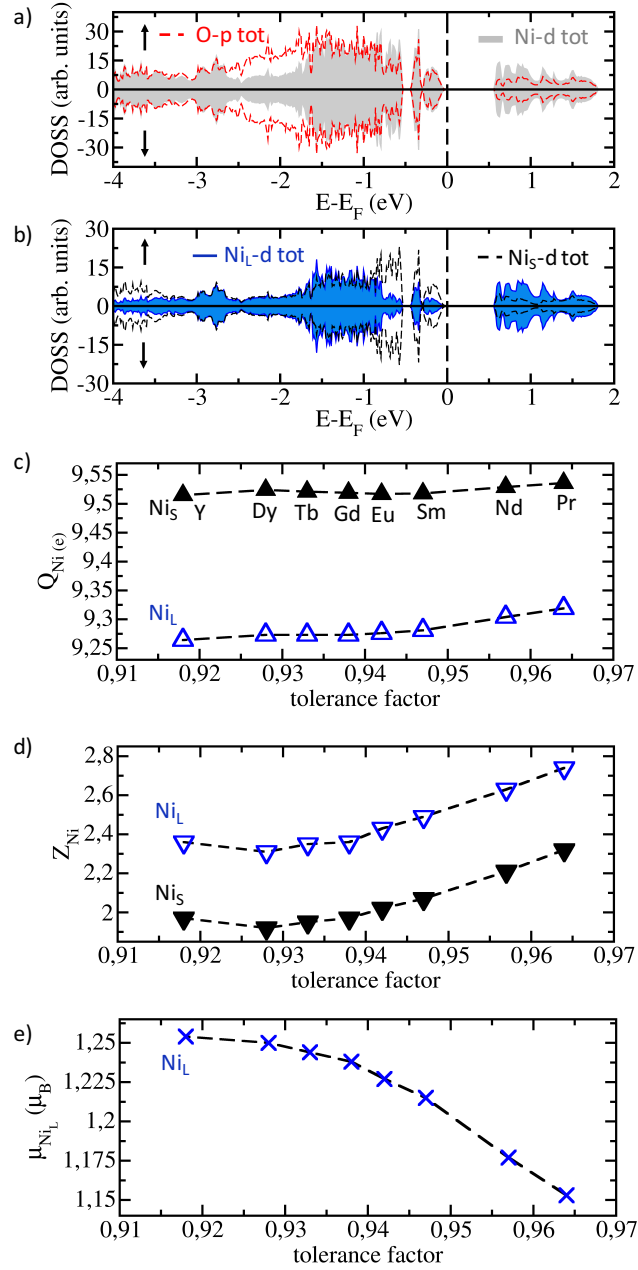


FIG. 3. **Key electronic properties of rare-earth nickelates ground state.** (a) and (b) Total and projected spin-polarized density of states (arbitrary units). The Fermi level is located at 0 eV. The upper (lower) panels correspond to spin up (down). (c) Total number of electrons ascribed to both Ni sites during the sphere integrations. (d) Average Born effective charges of both Ni sites. (e) Computed magnetic moment (in μ_B) of the Ni_L site. The magnetic moment of Ni_S is exactly zero in the calculation.

Disproportionation signatures

The electronic structure of the optimized ground states is characterized by strong hybridizations between O-2*p* and Ni-3*d* levels, as inferred from the projected density of states (pDOS, see Figure 3.a for the representative case of SmNiO₃). Comparing the pDOS corresponding to the 3*d* levels of the two different Ni sub-lattices reveals some small differences, likely reflecting weak disproportionation effects and a small charge ordering (see Figure 3.b). Although atomic charges are not uniquely defined in DFT calculations [39], sphere integrations around the Ni cations can provide some insight into the possible charge ordering. Figure 3.c reports the occupancy of both Ni sites as a function of the rare earth. A weak and rather constant charge ordering is observed between the Ni sites, going from $\delta=0.13$ (YNiO₃) to $\delta=0.11$ (PrNiO₃), but the sign of δ is opposite to what is expected. Indeed, the Ni_S cations, sitting at the center of the smallest O₆ octahedra, appear to hold more electrons than the Ni_L cations, located in the largest oxygen cages. Since the breathing mode B_{oc} enhances the crystal field splitting at the small NiO₆ groups, the *e_g* levels of Ni_S lie higher in energy than those of Ni_L [28, 40] and therefore Ni_S should have fewer electrons than Ni_L associated to it.

Let us now consider better defined – and experimentally measurable – quantities, such as Born effective charges (BECs) that measure the amount of charge displaced upon the movement of individual atoms. Figure 3.d reports the average of the diagonal components of the tensor for the different nickelates (see the Supplementary Material for the full tensors). In the representative case of SmNiO₃, we obtain $Z_{Ni_L} \approx +2.5$, which is not far from the nominal oxidation state of 2+ that this Ni site is associated with in the complete-charge-disproportionation picture. However, we find a similar $Z_{Ni_S} \approx +2.1$, which sharply deviates from the expectation value (4+) in the charge-disproportionation picture. As shown in Figure 3.d, we observe the same behavior across the various studied compounds; an approximately constant difference of Born charges, of about 0.4 electrons, is found across the whole series. Hence, from the point of view of the effective charges, the two Ni sites behave in a rather similar fashion, the disproportionation effects being weak and not complying with the usual picture.

However, our computed magnetic moments on both Ni sites appear to be in contradiction with the conclusion of the charge analysis. Indeed, as shown in Figure 3.e, we observe a

large difference between Ni_L – with a moment larger than $1 \mu_B$ – and Ni_S – for which the magnetic moment is null –, which suggests two very different electronic states.

Wannier analysis

The conclusion of the previous discussion is that, in the RNiO_3 compounds, all Ni atoms seem to display a similar oxidation state. Yet, the presence of a significant breathing distortion, and of the drastic difference in the local magnetic moments, clearly suggest two markedly different electronic states. Note that similar results have been reported in previous theoretical works using a variety of methods [25, 26, 30], but in our opinion a convincing explanation for this apparent contradiction is still missing. Here we ran a Wannier function (WF) analysis of our first-principles results, which allowed us to resolve this pending issue.

We used the Wannier90 package [41–43] to determine the maximally-localized WFs that reproduce the occupied electronic manifold. More precisely, our purpose was to count how many occupied WFs are centered at the different Ni cations, and how many at the surrounding oxygen anions, and to characterize them. Further, we wanted to run our analysis without having to make any assumption on the precise character of the occupied Ni and O orbitals, which complicated the choice of the seed functions that are needed for an efficient maximal-localization calculation. Nevertheless, we found the following robust strategy to proceed. We considered the whole occupied manifold and sought to extract from it (*i.e.*, to disentangle) a set of $2 \times (144 + 10)$ WF functions, where $2 \times 144 = 2 \times 3 \times 48$ is the total number of O- $2p$ orbitals available in our 80-atom supercell and $2 \times 10 = 2 \times 5 \times 2$ is the number of Ni- $3d$ orbitals corresponding to two specific Ni atoms. (Note that we ran separate WF optimizations for the spin-up and spin-down channels.) Hence, for our initial WF seeds, we used 3 generic p orbitals centered at each of the O anions in our cell, and 5 generic d orbitals centered at two neighboring Ni cations; this couple of Ni cations were chosen to be first-nearest neighbors, so that we considered one Ni_L and one Ni_S . The basic qualitative results of this optimization were the same for all the nickelates considered, and thus the following discussion is not compound specific.

Our optimization renders 2×3 WFs centered at each oxygen anion (*i.e.*, 3 spin-up WFs and 3 – very similar – spin-down WFs), suggesting that all oxygens in our nickelates are in a 2– oxidation state. The oxygen-centered WFs have a clear p character, as can be

appreciated in Figures 4.c and d. We also obtained 2×3 t_{2g} -like WFs centered at each of the two considered Ni atoms, indicating that the t_{2g} states are fully occupied and there is no magnetic moment associated to them. Further, we obtained 2 e_g -like spin-up WFs centered at the Ni_L site (see Figures 4.a and b), indicating that this cation is in a 2+ oxidation state and has a significant magnetic moment associated to it. Finally, as regards the other seed functions centered at the chosen Ni_L (2 spin-down d orbitals) and Ni_S (2×2 d orbitals) atoms, they did not lead to any WF centered at those sites. Instead, the maximal-localization procedure resulted in WFs centered at Ni and R cations in the vicinity of the considered Ni_L - Ni_S pair. Thus, in particular, it was impossible to localize any e_g -like WFs at a Ni_S site, which strongly indicates that these Ni cations are in a 4+ oxidation state. These conclusions were ratified by considering larger clusters of Ni sites for the WF optimization, as well as individual Ni's and/or optimizations in which the oxygen bands were not included.

Hence, the Wannier analysis yields a picture of strong charge disproportionation between the Ni sites, which is clearly at odds with the quantitatively similar behavior discussed in the section above. To resolve this apparent contradiction, we need to inspect in more detail the obtained oxygen-centered WFs.

Figures 4.c and d report representative results, for SmNiO_3 , of the O-2*p*-like Wannier functions oriented along the Ni-O-Ni bonds. As it is clearly visible in the figures for both spin channels, these WFs have their centers significantly shifted towards the Ni_S cations and away from the Ni_L sites. The shift – as quantified by the distance between the oxygen position and WF center – is ~ 0.231 Å in average. Hence, while the Ni_S cations appear to be in a 4+ state when we count how many WFs are centered at them, they also *receive* a significant fraction of electrons coming from the surrounding oxygens, with which they are strongly hybridized. Hence, this is the explanation why quantitative measures of the charge around the Ni_S ions renders results that are similar to those of the Ni_L and suggest valence state much more reduced than the expected 4+. Across the series, we observe that O-2*p* centers get closer to the Ni_S cations for smaller rare earths, increasing the localization of the charge on Ni_S . Additionally, the O-2*p* WFs behave similarly irrespective of their spin polarization, so that their shifting does not result in any magnetic moment at the Ni_S sites.

The Wannier analysis therefore leads to the conclusion that a full disproportionation occurs in the system, with clearly distinct Ni_S^{4+} (low-spin, non-magnetic) and Ni_L^{2+} (high-spin, magnetic) sites. Simultaneously, the O-2*p* WFs approach the Ni_S^{4+} sites, ultimately

yielding Ni_S and Ni_L that are nearly equivalent from the point of view of the charge (static and dynamics) around them.

DISCUSSION

Our results thus appear to be compatible with the disproportionation effects originally proposed to occur at the MIT [12–14]. While for a long time the nickelates were believed to possess an orthorhombic $Pbnm$ symmetry in the insulating phase [2], it is now established that they adopt a monoclinic $P2_1/n$ phase at low temperatures [12, 13]. This phase exhibits a breathing distortion whose magnitude decreases with increasing the tolerance factor of the perovskite [13], concomitantly accompanied by a charge disproportionation δ between the two Ni sites, leading to a $\text{Ni}_\text{S}^{(3+\delta)+} + \text{Ni}_\text{L}^{(3-\delta)+}$ configuration [14]. Our results are reminiscent of this picture, with the observation of a subsequent breathing distortion modulated by the rare earth and a charge disproportionation between Ni sites.

Nevertheless, they are also compatible with the model of Mizokawa *et al* [44], as well as with recent Dynamical Mean Field Theory (DMFT) studies [29, 30, 45–47], proposing a ligand-hole structure in rare-earth nickelates. Indeed, our Wannier analysis indicates that we have a $3d^8$ electronic configuration for the Ni_L cations. More importantly, it is also compatible with the $3d^8 \underline{L}^2$ configuration proposed for the Ni_S sites. More precisely, the notation \underline{L}^2 stands for the two oxygen holes that are shared by the oxygens in the O_6 octahedron surrounding a Ni_S cation. According to our Wannier analysis, such a situation would correspond to having all six oxygens around Ni_S sharing the $2p$ electrons that occupy orbitals along the Ni–O–Ni bonds. Further, given that our integrated and dynamical Born charges suggest that the Ni_S and Ni_L sites host a similar number of electrons, our results do in fact point to a situation in which each O_6 cage shares approximately two electrons with the Ni_S at its center, exactly as in the ligand-hole picture.

As regards the magnetic moments at the different Ni sites, our results are also clear and compatible with both proposed pictures: Ni_L bears a magnetic moment approaching $2 \mu_B$, as it corresponds to having Ni^{2+} in a high-spin configuration. Then, Ni_S has no magnetic moment associated to it, as it would correspond to a nominal Ni^{4+} low-spin configuration. The latter result is partly a consequence of the fact that the oxygen– Ni_S shared electrons are spin paired, which can be interpreted as a ligand-hole screening.

Our first-principles calculations therefore reconcile the two visions proposed to occur in the ground state of rare-earth nickelates. The electronic structure is summarized in Figure 4.e and is based on having i) a full charge disproportionation between Ni_L and Ni_S sites accompanied by a breathing mode and ii) 2 electrons from surrounding oxygens shared with the depleted Ni_S site, leaving the impression of two similar Ni^{2+} sites in the system. Finally, this electronic structure lifts the orbital degeneracy appearing in the high temperature phase and is compatible with the small Jahn-Teller distortion observed in our computed ground states.

Although the electronic structure is similar between all nickelates, the rare-earth cation does have an impact on the level of covalency of the system through their induced lattice distortions. An example is their influence on the magnetic moment of the Ni_L cations. Note that our computed Ni_L magnetic moments are always far from the nominal value of $2\mu_B$, as a consequence of the the hybridization between Ni-3d and O-2p states. This can be seen in Figures 4.c and d where slightly larger overlaps between O-2p orbitals over the Ni_L site arise in the spin up channel (this Ni_L site has a net spin up). From Figure 3.e, the level of covalency clearly increases with the tolerance factor (a ferromagnetic calculation yields similar conclusion, see Supplementary Material). This is further confirmed by the increase of the average BECs on both Ni_S and Ni_L following their interpretation of such effects in other perovskite oxides [48]. We also observe increasing O-2p overlaps with Ni_L sites going from R=Y to Pr.

The level of covalency seems to correlate with the stability of the magnetic ordering and the insulating phase (see Table I). On one hand, with increasing covalency, the energy difference between the AFM (S or T) and FM solutions increases strongly. On the other hand, the insulating gap decreases. In order to further corroborate these trends, we performed additional calculations on SmNiO_3 by applying a hydrostatic pressure of $\pm 8\%$ on the ground state volume and relaxed the atomic positions for each magnetic ordering. Under compression, we find a sizable enhancement of the covalent character as μ_{Ni_L} decreases to $1.103 \mu_B$. The stability of the S-AFM ordering with respect to the FM solution is therefore doubled ($\Delta E = -293$ meV per 80-atom cell). Eventually, the band gap is decreased by 0.11 eV with respect to the ground state value. Under expansion, we observe a weakening of the covalent character of the system with μ_{Ni_L} increasing to $1.308 \mu_B$; simultaneously, the stability of the complex AFM ordering is roughly reduced by a factor of 2 ($\Delta E = -67$ meV per 80-atom

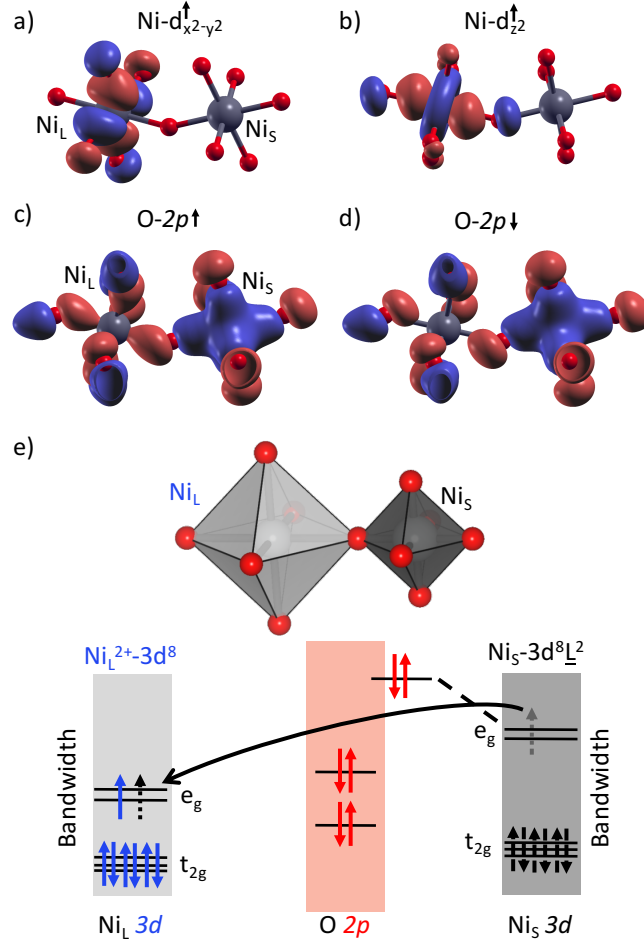


FIG. 4. **Orbital occupancies in rare-earth nickelates.** (a) $d_{x^2-y^2}^{\uparrow}$ max localized Wannier function on two consecutive Ni sites. The Ni_L site bears a spin up. (b) $d_{z^2}^{\uparrow}$ max localized Wannier function on two consecutive Ni sites. The Ni_L site bears a spin up. (c) $\text{O-}2p$ max localized Wannier functions oriented along the Ni-O bonds on the two consecutive Ni sites in the spin up channel. (d) $\text{O-}2p$ max localized Wannier functions oriented along the Ni-O bonds on the two consecutive Ni sites in the spin down channel. (e) Schematic picture of the electronic structure of rare-earth nickelates ground state.

cell).

Finally, the rare-earth atom is known to play key role in the nature of the MIT. Experimentally it is observed that T_{MI} is different from the magnetic-ordering transition temperature T_{N} for all nickelates except for those in which the rare earth is Pr or Nd. Interestingly, our calculations reflect this differentiated behavior. As already mentioned, we obtain an

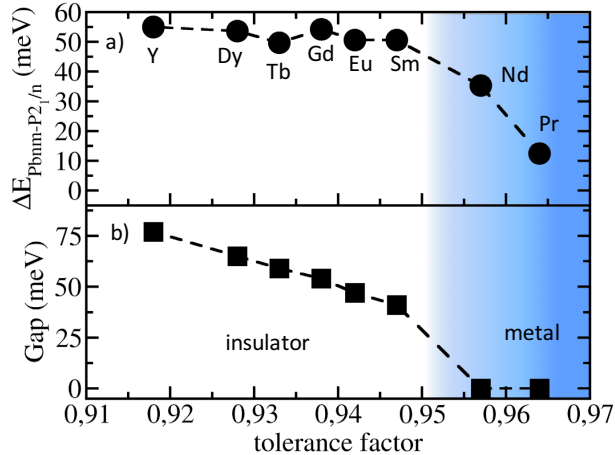


FIG. 5. **Metal-insulator phase transition** (a) Energy difference (in meV) per 20 atoms unit cell between the relaxed monoclinic and orthorhombic phases for a ferromagnetic solution; (b) Band gap (in meV) of the ferromagnetic monoclinic phase.

insulating solution for the AFM monoclinic ground state of all considered nickelates. Then, when we consider the $P2_1/n$ structure with a ferromagnetic spin arrangement, we also obtain an insulating phase for all R cations ranging from Y to Sm; the corresponding band gaps range from 77 to 41 meV and we observe a relatively large energy gain with respect to the orthorhombic phase (see Figures 5.a and b). Thus, the breathing distortion and disproportionation effects seem sufficient to open the band gap in these compounds, irrespective of the spin arrangement. As a consequence, our results indicate that these nickelates can potentially present an insulating, spin-disordered phase, as they indeed do experimentally. In contrast, for the monoclinic phase of NdNiO_3 and PrNiO_3 , the FM spin configuration is found to be metallic; further, the stability of the low-symmetry structure with respect to the orthorhombic one drastically decreases. The complex antiferromagnetic ordering therefore appears to be a necessary condition for the MIT to occur in these two compounds.

Considering the case of SmNiO_3 under 8% of compression, we unveil a similar behaviour to bulk PrNiO_3 and NdNiO_3 , since the level of covalency increases. These results suggest that it is possible to control of the electronic and magnetic structures of these compounds by tuning the level of covalency in the system. We also emphasize that these observations again support our choice of a small Hubbard U correction on Ni-3d sites and demonstrate that DFT+U methods can capture the key physical properties of correlated systems.

In summary, we have used first-principles methods to investigate the ground state electronic structure of rare-earth nickelates. Our DFT simulations using a small Hubbard correction on Ni-3*d* states reproduce all features reported from experiments (insulating character, disproportionation effects, covalency, complex antiferromagnetic structures, structural trends). In particular, we show that the insulating phase is characterized by a clear-cut split of the electronic states of the two Ni sites, which can be strictly described as being low-spin 4+ and high-spin 2+. At the same time, our simulations reveal a shift of the oxygen-*p* orbitals toward the depleted Ni cations, so that, ultimately, from the point of view of the integrated charge, the two Ni sites appear to be nearly identical. These findings are clearly reminiscent of the various pictures proposed in the literature to explain the ground state of these compounds, which can thus be reconciled according to our results. Finally, we unveil that a control of the level of covalency between oxygens and transition metal ions provides an alternative pathway to tune the electronic and magnetic phases in late transition-metal oxide perovskites.

METHODS

First-principles calculations were performed with the Vienna Ab-initio Simulation Package (VASP) package [49, 50]. Magnetism was treated only at the collinear level. We used a $3 \times 6 \times 2$ Γ -centered K-point mesh. The cut-off was set to 500 eV. We used PAW pseudopotentials [51] with the following electron configurations: $4s^2 3d^8$ (Ni), $2s^2 2p^4$ (O), $4s^2 4p^6 5s^2 4d^1$ (Y), $4s^2 4p^6 5s^2 4f^1$ (Pr, Nd, Sm), $4p^6 5s^2 4f^1$ (Gd, Eu, Tb, Dy). We did not treat explicitly the *f* electrons as they order at very low temperature [52] and they were included in the pseudopotential. Full geometry relaxations were performed until forces were lower than 0.001 eV/Å and energy was converged to 1×10^{-7} eV. Born Effective Charges were computed using density functional perturbation theory [53]. Symmetry adapted modes allowing the extraction of lattice distortion amplitudes were performed using the Bilbao crystallographic server [54, 55]. The results presented in Figures 2.d, e and f have been obtained by freezing single lattice distortion in a cubic reference that has the same lattice parameters for all nickelates. Wannier functions reported in Figures 4.a and b are plotted for isosurfaces equal to 2. Wannier functions reported in Figures 4.c and d are plotted for isosurfaces equal to 9.

ACKNOWLEDGMENTS

Work supported by the ERC grant MINT (contract #615759) and by National Research Fund, Luxembourg through a Pearl Grant (FNR/P12/4853155). J. Varignon acknowledges Ph. Ghosez and A. Mercy for fruitful discussions.

* julien.varignon@thalesgroup.com

- [1] Zubko, P., Gariglio, S., Gabay, M., Ghosez, P. & Triscone, J. M. Interface physics in complex oxide heterostructures. *Annu. Rev. Condens. Matter Phys.* **2**, 141-165 (2011).
- [2] Medarde, M. L. Structural, magnetic and electronic properties of RNiO₃ perovskites (R= rare earth). *J. Phys.: Condens. Matter* **9**, 1679-1707 (1997).
- [3] Catalan, G. Progress in perovskite nickelate research. *Phase Transitions* **81**, 729-749 (2008).
- [4] Boris, A. V., Matiks, Y., Benckiser, E., Frano, A., Popovich, P., Hinkov, V., Wochner, P., Castro-Colin, M., Detemple, E., Malik, V. K., Bernhard, C., Prokscha, T., Suter, A., Salman, Z., Morenzoni, E., Cristiani, G., Habermeier, H.-U. & Keimer, B. Dimensionality control of electronic phase transitions in nickel-oxide superlattices. *Science* **332**, 937-940 (2011).
- [5] Giovannetti, G., Kumar, S., Khomskii, D., Picozzi, S. & Van den Brink, J. Multiferroicity in Rare-Earth Nickelates RNiO₃. *Phys. Rev. Lett.* **103**, 156401 (2009).
- [6] Zhao, H. J., Ren, W., Yang, Y., Ñíguez, J., Chen, X. M. & Bellaiche, L. Near room-temperature multiferroic materials with tunable ferromagnetic and electrical properties. *Nat. Commun.* **5**, 4021 (2014).
- [7] Chaloupka, J. & Khaliullin, G. Orbital order and possible superconductivity in LaNiO₃/LaMO₃ superlattices. *Phys. Rev. Lett.* **100**, 016404 (2008).
- [8] Grisolia, M. N., Varignon, J., Sanchez-Santolino, G., Arora, A., Valencia, S., Varela, M., Abrudan, R., Weschke, E., Schierle, E., Rault, J. E., Rueff, J. P., Barthélemy, A., Santamaria J. & Bibes, M. Hybridization-controlled charge transfer and induced magnetism at correlated oxide interfaces. *Nat. Phys.* , 3627 (2016).
- [9] Gibert, M., Zubko, P., Scherwitzl, R., Ñíguez, J. & Triscone, J. M. Exchange bias in LaNiO₃-LaMnO₃ superlattices. *Nat. Mater.* **11** , 195-198 (2012).

- [10] Benckiser, E., Haverkort, M. W., Brück, S., Goering, E., Macke, S., Frañó, A., Yang, X., Andersen, O. K., Cristiani, G., Habermeier, H.-U., Boris, A. V., Zegkinoglou, I., Wochner, P., Kim, H. J., Hinkov, V. & Keimer, B. Orbital reflectometry of oxide heterostructures. *Nat. Mater.* **10**, 189-193 (2011).
- [11] Hepting, M., Minola, M., Frano, A., Cristiani, G., Logvenov, G., Schierle, E., Wu, M., Bluschke, M., Weschke, E., Habermeier, H.-U., Benckiser, E., Le Tacon, M., & Keimer B. Tunable Charge and Spin Order in PrNiO₃ Thin Films and Superlattices. *Phys. Rev. Lett.* **113**, 227206 (2014).
- [12] Alonso, J. A., Martínez-Lope, M. J., Casais, M. T., Aranda, M. A. & Fernández-Díaz, M. T. Metal-insulator transitions, structural and microstructural evolution of RNiO₃ (R= Sm, Eu, Gd, Dy, Ho, Y) perovskites: Evidence for room-temperature charge disproportionation in monoclinic HoNiO₃ and YNiO₃ *J. Am. Chem. Soc.* **121**, 4754-4762 (1999).
- [13] Medarde, M. L., Fernández-Díaz, M. & Lacorre, P. Long-range charge order in the low-temperature insulating phase of PrNiO₃. *Phys. Rev. B* **78**, 212101 (2008).
- [14] Medarde, M., Dallera, C., Grioni, M., Delley, B., Vernay, F., Mesot, J., Sikora, M., Alonso, J. & Martínez-Lope, M. Charge disproportionation in RNiO₃ perovskites (R= rare earth) from high-resolution x-ray absorption spectroscopy. *Phys. Rev. B* **80**, 245105 (2009).
- [15] García-Muñoz, J., Rodríguez-Carvajal, J. & Lacorre, P. Neutron-diffraction study of the magnetic ordering in the insulating regime of the perovskites RNiO₃ (R= Pr and Nd). *Phys. Rev. B* **50**, 978 (1994).
- [16] Rodríguez-Carvajal, J., Rosenkranz, S., Medarde, M. L., Lacorre, P., Fernández-Díaz, M., Fauth, F. & Trounov, V. Neutron-diffraction study of the magnetic and orbital ordering in ¹⁵⁴SmNiO₃ and ¹⁵³EuNiO₃. *Phys. Rev. B* **57**, 456 (1998).
- [17] García-Muñoz, J., Rodríguez-Carvajal, J. & Lacorre, P. Sudden appearance of an unusual spin density wave at the metal-insulator transition in the perovskites RNiO₃ (R= Pr, Nd). *Europhys. Lett.* **20**, 241 (1992).
- [18] Bodenthin, Y., Staub, U., Piamonteze, C., García-Fernández, M., Martínez-Lope, M. & Alonso, J. Magnetic and electronic properties of RNiO₃ (R= Pr, Nd, Eu, Ho and Y) perovskites studied by resonant soft X-ray magnetic powder diffraction *J. Phys.: Condens. Matter* **23**, 036002 (2011).

- [19] Torrance, J.B., Lacorre, P., Nazzal, A. I., Ansaldo, E. J. & Niedermayer, C. Systematic study of insulator-metal transitions in perovskites RNiO_3 (R= Pr, Nd, Sm, Eu) due to closing of charge-transfer gap. *Phys. Rev. B* **45**, 8209-8212 (1992).
- [20] Obradors, X., Paulius, L., Maple, M., Torrance, J., Nazzal, A., Fontcuberta, J. & Granados, X. Pressure dependence of the metal-insulator transition in the charge-transfer oxides RNiO_3 (R= Pr, Nd, $\text{Nd}_{0.7}\text{La}_{0.3}$). *Phys. Rev. B* **47**, 12353-12356 (1993).
- [21] Canfield, P., Thompson, J., Cheong, S. & Rupp, L. Extraordinary pressure dependence of the metal-to-insulator transition in the charge-transfer compounds NdNiO_3 and PrNiO_3 . *Phys. Rev. B* **47**, 12357-12360 (1993).
- [22] Zhou, J. S., Goodenough, J. & Dabrowski, B. Pressure-induced non-Fermi-liquid behavior of PrNiO_3 . *Phys. Rev. Lett.* **94**, 226602 (2005).
- [23] Scherwitzl, R., Zubko, P., Lezama, I. G., Ono, S., Morpurgo, A. F., Catalan, G. & Triscone, J. M. Electric-Field Control of the Metal-Insulator Transition in Ultrathin NdNiO_3 Films. *Adv. Mater.* **22**, 5517-5520 (2010).
- [24] He, Z. & Millis, A. J. Strain control of electronic phase in rare-earth nickelates. *Phys. Rev. B* **91**, 195138 (2015).
- [25] Bruno, F. Y. , Rushchanskii, F. Y. , Valencia, S., Dumont, Y., Carrétéro, C., Jacquet, E., Abrudan, R., Blügel, S., Ležaić, M. Bibes, M. & Barthélémy, A. Rationalizing strain engineering effects in rare-earth nickelates. *Phys. Rev. B* **88**, 195108 (2013).
- [26] Prosandeev, S., Bellaiche, L. & Íñiguez, J. *Ab initio* study of the factors affecting the ground state of rare-earth nickelates. *Phys. Rev. B* **85**, 214431 (2012).
- [27] Yamamoto, S. & Fujiwara, T. Charge and spin order in RNiO_3 (R= Nd, Y) by LSDA+U method. *J. Phys. Soc. Jpn.* **72**, 1226-1229 (2002).
- [28] Mazin, I., Khomskii, D., Lengsdorf, R., Alonso, J., Marshall, W., Ibberson, R., Podlesnyak, A., Martinez-Lope, M. & Abd-Elmeguid, M. Charge ordering as alternative to Jahn-Teller distortion. *Phys. Rev. Lett.* **98**, 176406 (2007).
- [29] Peil, O. E. & Georges, A. Low-energy description of the metal-insulator transition in the rare-earth nickelates. *Phys. Rev. B* **91**, 075128 (2015).
- [30] Park, H., Millis, A. J., Marianetti, C. A. Site-selective Mott transition in rare-earth-element nickelates. *Phys. Rev. Lett.* **109**, 156402 (2012).

- [31] Perdew, J. P. , Ruzsinszky, A., Csonka, G. I., Vydrov, O. A., Scuseria, G. E., Constantin, L. A., Zhou, X. & Burke, K. Restoring the Density-Gradient Expansion for Exchange in Solids and Surfaces. *Phys. Rev. Lett.* **100**, 136406 (2008).
- [32] Liechtenstein, A. I., Anisimov, V. I. & Zaanen, J. Density-functional theory and strong interactions: Orbital ordering in Mott-Hubbard insulators. *Phys. Rev. B* **52**, 5467(R) (1995).
- [33] Arima, T., Tokura, Y. & Torrance, J. B. Variation of optical gaps in perovskite-type 3d transition-metal oxides. *Phys. Rev. B* **48**, 17006-17009 (1993).
- [34] Mizokawa, T., Fujimori, A., Arima, T., Tokura, Y., Mōri, N. & Akimitsu, J. Electronic structure of PrNiO₃ studied by photoemission and x-ray-absorption spectroscopy: Band gap and orbital ordering. *Phys. Rev. B* **52**, 13865 (1995).
- [35] We have also considered usual A, C and G-type AFM orderings but these solutions are always found higher in energy than the FM state by at least 400 meVs.
- [36] The gap is eventually reduced to 91 meV without Coulombic correction on the Ni 3d states.
- [37] Glazer, A. The classification of tilted octahedra in perovskites. *Acta Crystallogr., Sect. B: Struct. Crystallogr. Cryst. Chem.* **28**, 3384-3392 (1972).
- [38] V. M. Goldschmidt, V. M. Die gesetze der krystallochemie. *Naturwissenschaften* **14**, 477-485 (1926).
- [39] Quan, Y., Pardo, V. & Pickett, W. E. Formal Valence, 3d-Electron Occupation, and Charge-Order Transitions. *Phys. Rev. Lett.* **109**, 216401 (2012). 216401.
- [40] Bristowe, N. C., Varignon, J., Fontaine, D., Bousquet, E. & Ghosez, P. Ferromagnetism induced by entangled charge and orbital orderings in ferroelectric titanate perovskites. *Nat. Commun.* **6**, 6677 (2015).
- [41] Mostofi, A. A., Yates, J. R., Lee, Y. S., Souza, I., Vanderbilt, D. & Marzari, N. Wannier90: A tool for obtaining maximally-localised Wannier functions. *Comput. Phys. Commun.* **178**, 685-699 (2008).
- [42] Marzari, N. & Vanderbilt, D. Maximally localized generalized Wannier functions for composite energy bands. *Phys. Rev. B* **56**, 12847-12865 (1997).
- [43] Souza, I., Marzari, N. & Vanderbilt, D. Maximally localized Wannier functions for entangled energy bands. *Phys. Rev. B* **65**, 035109 (2001).
- [44] Mizokawa, T., Khomskii, D. & Sawatzky, G. Spin and charge ordering in self-doped Mott insulators. *Phys. Rev. B* **61**, 11263-11266 (2000).

- [45] Ruppen, J., Teyssier, J., Peil, O. E., Catalano, S., Gibert, M., Mravlje, J., Triscone, J. M., Georges, A. & van der Marel, D. Optical spectroscopy and the nature of the insulating state of rare-earth nickelates. *Phys. Rev. B* **92**, 155145 (2015).
- [46] Lau, B. & Millis, A. J. Theory of the Magnetic and Metal-Insulator Transitions in RNiO_3 Bulk and Layered Structures. *Phys. Rev. Lett.* **110**, 126404 (2013).
- [47] Park, H., Millis, A. J. & Marianetti, C. A. Total energy calculations using DFT+DMFT: Computing the pressure phase diagram of the rare earth nickelates. *Phys. Rev. B* **89**, 245133 (2014).
- [48] Ghosez, P., Gonze, X., Lambin, P. & Michenaud, J. P. Born effective charges of barium titanate: Band-by-band decomposition and sensitivity to structural features. *Phys. Rev. B* **51**, 6765-6768 (1995).
- [49] Kresse, G. & Haffner, J. Ab initio molecular dynamics for liquid metals. *Phys. Rev. B* **47**, 558-561 (1993).
- [50] Kresse, G. & Furthmüller, J. Efficiency of ab-initio total energy calculations for metals and semiconductors using a plane-wave basis set. *Comput. Mater. Sci.* **6**, 15-50 (1996).
- [51] Blöchl, P. E. Projector augmented wave method. *Phys. Rev. B* **50**, 17953-17979 (1994).
- [52] Fernández-Díaz, M., Alonso, J., Martínez-Lope, M., Casais, M. & García-Muñoz, J. Magnetic structure of the HoNiO_3 perovskite. *Phys. Rev. B* **64**, 144417 (2001).
- [53] Baroni, S., de Gironcoli, S., Dal Corso, A. & Giannozzi, P. Phonons and related crystal properties from density-functional perturbation theory. *Rev. Mod. Phys.* **73**, 515-562 (2001).
- [54] Orobengoa, D., Capillas, C., Aroyo, M. I. & Perez-Mato, J. M. AMPLIMODES: symmetry-mode analysis on the Bilbao Crystallographic Server. *J. Appl. Crystallogr.* **42**, 820-833 (2009).
- [55] Perez-Mato, J. M., Orobengoa, D. & Aroyo, M. Mode crystallography of distorted structures. *Acta Crystallogr., Sect. A: Found. Crystallogr.* **66**, 558-590 (2010).